Available online at www.sciencedirect.com
SCIENCE DIRECT®
Journal of Sound and Vibration 273 (2004) 337–361
JOURNAL OF SOUND AND VIBRATION
www.elsevier.com/locate/jsvi

Non-linear free vibration of a cable against a straight obstacle

S.M. Han*, M.A. Grosenbaugh

Applied Ocean Physics and Engineering Department, Woods Hole Oceanographic Institution, Woods Hole, MA 02543, USA

Received 20 November 2002; accepted 22 April 2003

Abstract

The goal of this study was to show how the response of a cable was altered after it impacted a straight obstacle. The two ends of the cable were held at the same level, and the cable was initially vibrating at its first symmetric mode. The free vibration of a cable depends on the amplitude of vibration, the sag-to-span ratio, and the ratio of the elastic to geometric stiffness as measured by Irvine and Caughey's cable parameter λ^2. How these variables affected the response of a cable interacting with a straight obstacle was examined for three limiting cases: a nearly taut string, an extensible shallow-sag cable, and an inextensible deep-sag cable. For a nearly taut string interacting with a straight obstacle in the absence of gravity, the periodicity that occurs for a linear taut string was preserved even when the amplitude of vibration was large. However, the frequency of vibration was modified due to the non-linear effects of large amplitudes. The periodicity was lost if the cable was not taut both in the presence and in the absence of gravity. For the case of a nearly taut string with gravity, the periodicity could be recovered if the obstacle assumed the shape of the equilibrium configuration of the cable. This was because the obstacle no longer behaved as a straight obstacle but as a convex obstacle whose radius of curvature decreased with decreasing amplitude-to-sag ratio. The behavior approached that of a point obstacle in the limit. Shallow-sag cables were analyzed by keeping the amplitude-to-sag ratio constant so that the obstacle behaved in a consistent manner. Comparison of our findings with the results of Irvine and Caughey for the free vibrations of a cable in air showed that the relative frequency based on the time to the first contact was not affected by the presence of the obstacle for all values of λ^2. However, the relative frequency based on the time between the first two contacts was slightly reduced when compared to the values corresponding to a non-interacting cable. This was attributed to the longer persistent contact that developed between the cable and the obstacle. Similar results were found for an inextensible deep-sag cable with various sag-to-span ratios. In both cases of shallow- and deep-sag cables, the ratio of the initial amplitude to the distance between the cable and the obstacle had a minimal effect on the reduction in the relative frequency.

*Corresponding author. Tel.: +1-508-289-3714; fax: +1-508-457-2191.
E-mail addresses: seonhan@whoi.edu (S.M. Han), mgrosenbaugh@whoi.edu (M.A. Grosenbaugh).

0022-460X/03/$ - see front matter
doi:10.1016/S0022-460X(03)00542-X

1. Introduction

The purpose of this study is to investigate the non-linear effects of varying amplitude and gravity on a cable vibrating against a straight obstacle. This problem has a number of practical applications including ocean mooring lines interacting with the sea bottom due to motion of a surface buoy, marine risers contacting each other due to vortex-induced vibrations, and "catch" wires hitting the deck of an aircraft carrier when a plane lands.

Cabannes [1] obtained the analytical solution for the simpler case of a linear taut string (with no gravity) transversely vibrating in the presence of a straight obstacle. He found that, if the string is allowed to hit the obstacle, the dynamic response is altered in a way that is related to the ratio h/A_0, where h is the distance from the obstacle to the equilibrium position of the string, and A_0 is the amplitude of a unimodal initial displacement (Fig. 1(a)). Contact occurs between the string and the obstacle when $h/A_0 \leqslant 1$. Cabannes [1] showed that, if h/A_0 can be represented by a rational number p/q (where p and q are the lowest integers), the motion is periodic with a period $(p+q)/2$ times the period of a freely vibrating string. On the other hand, the motion is nearly periodic if h/A_0 is irrational.

The linear string model assumes that the tension is assumed constant along the string's length and constant with time, and the natural frequencies are constant for a given cable. This assumption is valid if the amplitude of the motion and the equilibrium curvature due to gravity are small. If these conditions are not met, the coupling between the in-plane transverse and the longitudinal motion becomes important, and the dynamics need to be represented by the 2D cable equations [2,3]. We will use the term, "cable," to generally refer to a long and thin flexible body with no bending stiffness.

The natural frequencies and the mode shapes of a freely vibrating cable in air depend on the amplitude of vibration, the ratio of elastic-to-geometrical stiffness, and the ratio of equilibrium sag to span. The question of how these natural frequencies vary from those of a linear taut string has been investigated by number of researchers. For example, the effect of large amplitude was first investigated by Carrier [2,3]. Carrier started with a set of non-linear cable equations, which dates back to Euler (see Ref. [4]), and gave a perturbation solution in terms of amplitude. Hagedorn and Schafer [5] included gravity while limiting the analysis to a shallow-sag cable. They showed the variation in the natural frequency with the amplitude of the vertical displacement using the assumed mode method. Takahashi and Konishi [6] significantly expanded the previous

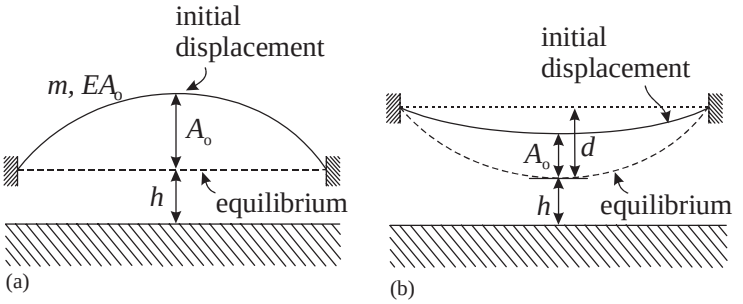

Fig. 1. Cables vibrating against straight obstacles: (a) zero gravity, (b) non-zero gravity.

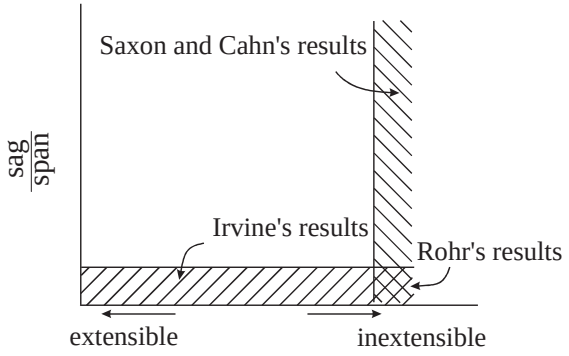

Fig. 2. The regions where the theories of Irvine and Caughey [9] and Saxon and Cahn [14] are valid.

work by considering inclined as well as horizontal cables. Their analysis included three dimensions and was not limited to small sag-to-span ratios.

The effect of the elastic and geometrical stiffness on the natural frequencies of a shallow-sag cable was shown independently by Simpson [7], West and Geschwindner [8], and Irvine and Caughey [9]. The limiting case of an inextensible cable with a shallow sag was investigated by Rohrs [10]. Triantafyllou [11] expanded the analysis to an inclined cable.

Finally, the effect of sag on the natural frequencies has been demonstrated almost exclusively by studies of inextensible cables. These include Routh [12], Pugsley [13], and Saxon and Cahn [14]. The range of dynamic behavior, covered by these results, spans the shallow-sag case of an almost inextensible cable to the extreme deep-sag case of a vertically hanging chain.

In this paper, we extend the non-linear analysis of the free vibration of a cable to include interaction with a straight obstacle. We investigate the effect of large amplitude on the taut-string result of Cabannes and also examine how the shallow- and deep-sag results are affected by the presence of the obstacle. We do this by first deriving a set of non-linear equations in two dimensions, which we solve numerically. For this study, we will restrict the ratio h/A_0 to $\frac{1}{2}$ and $\frac{1}{3}$. Also, we only look at the first symmetric mode. That is, the initial displacements must resemble the first mode shape. The mode shapes for a shallow-sag cable are taken from Irvine and Caughey [9] and for an inextensible cable from Saxon and Cahn [14]. Fig. 2 shows the regions where their results are valid. It should be noted that the unshaded region represents a highly extensible cable with a large sag such as a slinky. Such cables are rarely used in practice as load-carrying members. Therefore, it is sufficient to look only at the limiting cases.

2. Mathematical formulation

There are many different ways to formulate the non-linear cable equations. For our purposes, the equations of motion must be such that they can capture the non-linear effects of large amplitude, the ratio of elastic to geometrical stiffness, and the equilibrium sag. In this section, we will derive a set of fully non-linear equations of motion for a cable that is similar to the ones used by Perkins and Mote [15] and Han and Benaroya [16]. The finite strain model is used to capture the geometric non-linearities, which are important when the vibration amplitude and the

curvature is large. Two perpendicular displacements are used as dependent variables. The equations of motion are derived using Hamilton's principle. The equations of motion are such that the horizontal and vertical motions are non-linearly coupled.

Dimensional variables are denoted with a superscript $*$. For instance, the two displacements, $U^*(X^*, t^*)$ and $V^*(X^*, t^*)$, are the displacements of the central line of the cable in the global Cartesian co-ordinates measured from the original location in the horizontal and vertical directions as shown in Fig. 3. L^* is the length of the undeformed cable and l^* is the span or the length between the two ends. X^* is the Lagrangian co-ordinate, and x^* is the horizontal co-ordinate of the cable element X^*. They are related by

$$x^*(X^*, t^*) = X^* + U^*(X^*, t^*). \tag{1}$$

X^* ranges from 0 to L^*, and x^* ranges from 0 to l^*. The displacements are normalized by L^* such that

$$U = U^*/L^*, \quad V = V^*/L^*, \quad X = X^*/L^*, \quad x = x^*/L^*, \quad l = l^*/L^*. \tag{2}$$

The list of dimensional and non-dimensional variables is given in Appendix B.

The strain energy is defined by

$$PE^*_{strain} = \int_{V_0} \int_{\varepsilon^*} \sigma^*_{ij} \, \mathrm{d}\varepsilon^*_{ij} \, \mathrm{d}V^*_0 = \frac{1}{2} \int_{V_0} \sigma^*_{ij} \varepsilon^*_{ij} \, \mathrm{d}V^*_0, \tag{3}$$

where V^*_0 is the volume of the undeformed cable, σ^*_{ij} is the second Piola–Kirchhoff stress and ε^*_{ij} is the Green's strain. In our case, σ^*_{11} is the only non-zero stress and is related to the axial strain by $\sigma^*_{11} = E^* \varepsilon^*_{11}$, where E^* is Young's modulus and ε^*_{11} is the normal strain. In short, we will denote it as ε^*. Green's strain, ε^*, is defined by

$$\varepsilon^*(X, t) = \frac{\partial U^*}{\partial X^*} + \frac{1}{2}\left(\left(\frac{\partial U^*}{\partial X^*} \right)^2 + \left(\frac{\partial V^*}{\partial X^*} \right)^2 \right). \tag{4}$$

Note that the strain is already non-dimensional since the displacements and X are normalized by the same variable. Since U^* and V^* are functions of X^* and t^*, so is ε^*. Then, the strain energy

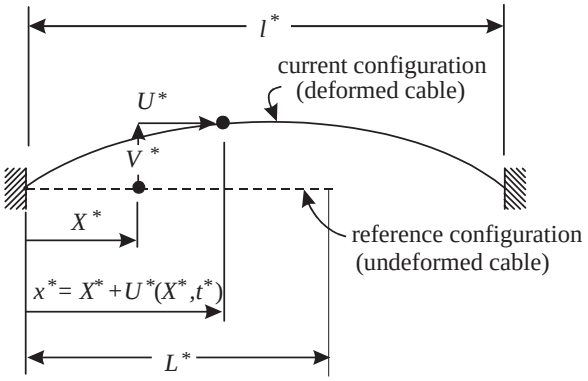

Fig. 3. Lagrangian co-ordinate X and two perpendicular displacements.

can be written as

$$PE^*_{strain} = \frac{1}{2}\int_0^{L^*} E^* A_0^* \varepsilon^{*2}\,\mathrm{d}X^*, \tag{5}$$

where A_0^* is the cross-sectional area of the undeformed cable. We normalize the energy by $E^* A_0^* L^*$ such that the strain energy becomes

$$PE_{strain} = \frac{1}{2}\int_0^1 \left(U' + \tfrac{1}{2}(U'^2 + V'^2)\right)^2 \mathrm{d}X, \tag{6}$$

where primes indicate differentiation with respect to X. The normalized potential energy due to gravity is given by

$$PE_{gravity} = \int_0^1 GV(X,t)\,\mathrm{d}X, \tag{7}$$

where G is the ratio of the total weight of the cable to the elastic stiffness and is given by

$$G = m^* g^* L^* / E^* A_0^*. \tag{8}$$

The non-conservative work done on the system by forces per unit length, $p_u(X,t)$ and $p_v(X,t)$, is given by

$$work_{nc} = \int_0^1 [p_u U + p_v V]\,\mathrm{d}X, \tag{9}$$

where

$$p_u = p_u^* \frac{L^*}{E^* A_0^*}, \quad p_v = p_v^* \frac{L^*}{E^* A_0^*}. \tag{10}$$

The normalized kinetic energy is given by

$$KE = \frac{1}{2}\int_0^1 m[\dot{U}^2 + \dot{V}^2]\,\mathrm{d}X, \tag{11}$$

where m is the normalized mass per unit length,

$$m = m^* \frac{L^{*2}\bar{\omega}_1^{*2}}{E^* A_0^*}. \tag{12}$$

The time t^* and the frequency ω^* are normalized such that

$$t = t^* \bar{\omega}_1^* \quad \text{and} \quad \omega = \omega^* / \bar{\omega}_1^*, \tag{13}$$

where $\bar{\omega}_1^*$ is the first natural frequency of the linear transverse model. The first transverse frequency of the linear model is given by

$$\bar{\omega}_1^* = \sqrt{\frac{H_e^*}{m^*}\frac{L^*}{l^*}}\frac{\pi}{L^*}, \tag{14}$$

where H_e^* is the constant horizontal equilibrium tension, m^*L^*/l^* is the mass per unit horizontal length denoted as m_x^*. The horizontal equilibrium tension is given by

$$H_e^* = E^* A_0^* \varepsilon_e^* \left(1 + \frac{\partial U_e^*}{\partial X^*}\right), \tag{15}$$

where ε_e^* and U_e^* are equilibrium strain and the horizontal displacements, respectively. Then, we can rewrite m in Eq. (12) as

$$m = \pi^2 \frac{L^*}{l^*} \frac{H_e^*}{E^* A_0^*} = \pi^2 \frac{H_e}{l}, \tag{16}$$

where H_e is the normalized horizontal equilibrium tension.

By combining Eqs. (6), (7), (9), and (11), the Lagrangian is given by

$$\begin{aligned} \mathscr{L} &= \int_{t_i}^{t_f} (KE - PE + W_{nc})\, \mathrm{d}t \\ &= \int_{t_i}^{t_f} \int_0^1 \left[\left\{ \frac{m}{2}(\dot{U}^2 + \dot{V}^2) - \tfrac{1}{2}\varepsilon^2 - GV \right\} + \{p_u U + p_v V\} \right] \mathrm{d}X\, \mathrm{d}t, \end{aligned} \tag{17}$$

with the nonholonomic constraint

$$V(X,t) \geqslant y_{obstacle}, \tag{18}$$

where $y_{obstacle}$ is the normalized distance to the obstacle from the horizontal line connecting the two ends of the cable and is equivalent to $y_{obstacle} = -(h + d)$, where d is the normalized equilibrium sag, and h is the normalized depth of the obstacle (Fig. 1).

If we assume that there is no frictional force when the cable encounters the obstacle, the functional to be minimized is given by

$$\hat{\mathscr{L}} = \mathscr{L} - \tfrac{1}{2}\gamma P^2(X,t), \tag{19}$$

where γ is the penalty parameter. $P(X,t)$ is the penalty function given by

$$P(X,t) = \begin{cases} (y_{obstacle} - V(X,t)) & \text{for } y_{obstacle} > V(X,t) \\ 0 & \text{for } y_{obstacle} \leqslant V(X,t). \end{cases} \tag{20}$$

The use of the penalty function is equivalent to inserting an elastic foundation with stiffness γ, where the dimensional stiffness γ^* is normalized by $E^*A_0^*/L^{*2}$. The solution approaches the true solution as $\gamma \to \infty$. The Lagrange multiplier in this case is equivalent to $\lim_{\gamma\to\infty} \gamma P$. The Lagrange multiplier is also the reaction force exerted by the obstacle. Dean et al. [17] showed that this method creates a boundary layer near the obstacle with thickness of order $1/\gamma$.

The equations of motion in terms of normalized parameters are given by

$$m\ddot{U} - (\varepsilon(1 + U'))' = p_u, \tag{21}$$

$$m\ddot{V} - (\varepsilon V')' + G = \gamma(y_{obstacle} - V)^+ + p_v, \tag{22}$$

though for this study, we set p_u and p_v equal to zero. The possible boundary conditions are obtained from

$$[\varepsilon(1 + U')]\delta U|_0^1 = 0, \quad \varepsilon V' \delta V|_0^1 = 0. \tag{23}$$

In our case, the two ends are fixed such that

$$U(0,t)=0, \quad V(0,t)=0, \quad U(1,t)=l-1, \quad V(1,t)=0. \tag{24}$$

If l is greater than 1, the cable is stretched out. If l equals zero, the two ends overlap, and the problem is equivalent to that of a hanging chain.

The equations of motion (without external forcing and obstacle) and boundary conditions (Eqs. (21), (22) and (24)) depend on m, G, and l. Note that m in Eq. (16) depends on H_e, which can be obtained by solving the static equations. The static equations depend only on G and l. Then, m is a function of G and l. Therefore, the dynamic response depends on three quantities, G, l, and initial conditions.

3. Results and discussion

The normalized equations of motion and boundary conditions given in the previous section revealed that the natural frequencies depend only on G, l, initial conditions, and h. Recall that G is the ratio of the total weight to the longitudinal stiffness, l is the ratio of the distance between the two ends to the undeformed length of the cable, and h is the ratio of the minimum distance between the cable and the obstacle (Fig. 1(b)) to the undeformed length of the cable.

Because we are interested only in the first symmetric natural frequency, we supply initial displacements that resemble the first symmetric mode shapes,

$$U(X,0)=U_e(X)+A_0U_1(X), \quad V(X,0)=V_e(X)+A_0V_1(X), \quad \dot{U}(X,0)=\dot{V}(X,0)=0, \tag{25}$$

where A_0 is the initial vertical displacement at the midpoint. $U_1(X)$ and $V_1(X)$ are the first mode shapes as given by Irvine and Caughey for a shallow-sag cable and Saxon and Cahn for an inextensible cable (see Appendix A). The mode shapes are normalized such that the midpoint vertical displacement, $V_1(\frac{1}{2})$, is 1. The equilibrium displacements, U_e and V_e, are obtained by solving the static equations. In the absence of gravity, they are given by

$$U_e=(l-1)X, \quad V_e=0. \tag{26}$$

By fixing the shape of the initial displacement (Eqs. (25) and (26)), the natural frequencies now depend on G, l, A_0, and h. In addition, we will let $h=A_0/2$ or $A_0/3$. Then, the natural frequencies depend only on G, l, and A_0. Irvine [18] presented their results in terms of the sag-to-span ratio and a parameter λ^2, which is the ratio of the elastic to geometrical stiffness and is defined by Eqs. (A.1) and (A.2) in Appendix A. A pair of values for G and l corresponds to a unique pair of values for λ^2 and d/l. For each of these cases, then, the natural frequencies depend on λ^2, d/l, and A_0. In this section, we explore the effects of each of these parameters on the first symmetric frequency.

The non-linear equations of motion are solved numerically using a central difference in space with 401 nodes and the Runge–Kutta method of fourth and fifth order in time. The penalty parameter or the spring constant of the elastic foundation is chosen sufficiently large to keep the total energy relatively constant.

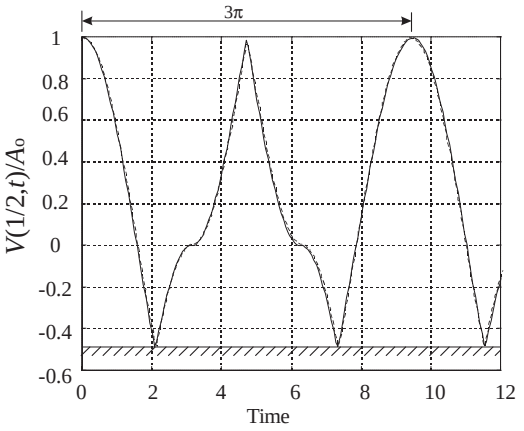

Fig. 4. Normalized vertical displacements at $X = \frac{1}{2}$, $V(\frac{1}{2}, t)$, where $G = 0$, $l = 1.05$, $A_0 = 0.01$, and $h/A_0 = \frac{1}{2}$: —, Cabannes; ⋯, non-linear PDE.

3.1. Comparison with Cabannes's results—no gravity

We will first show that the numerical solution of the present model can produce the analytical result obtained by Cabannes [1,19] for the limiting case when the cable behaves as a linear taut string and $G = 0$. Fig. 4 compares the vertical displacements at the midpoint of the cable obtained analytically by Cabannes and numerically by solving our present cable model. Here, we used $l = 1.05$, $A_0 = 0.01$, and $h/A_0 = \frac{1}{2}$. The figure shows a good agreement between the analytical and numerical solutions. The first natural frequency is very close to that of a linear taut string. Recall that the natural frequencies are normalized by the first natural frequency of a linear taut string so that the first natural frequency of a linear taut string is 1.

According to Cabannes, the period is modified such that

$$T = \frac{(p+q)}{2} T_n. \tag{27}$$

In our case, $p/q = \frac{1}{2}$ and the period of the motion is

$$period = \frac{1+2}{2} 2\pi = 3\pi, \tag{28}$$

which is confirmed by Fig. 4.

Fig. 5 shows the kinetic and potential energy obtained by solving the present cable model numerically. The expressions for potential and kinetic energy are given by Eqs. (6), (7) and (11). The integration is performed using a trapezoidal rule. The change in the total energy at $t = 12$ is -0.079% of the original value, which is very small. Therefore, the total energy can be considered conserved, and this verifies that the stiffness of elastic foundation ($\gamma = 10^8$) and shows that the number of nodes used here ($N = 401$) is adequate for providing an accurate solution.

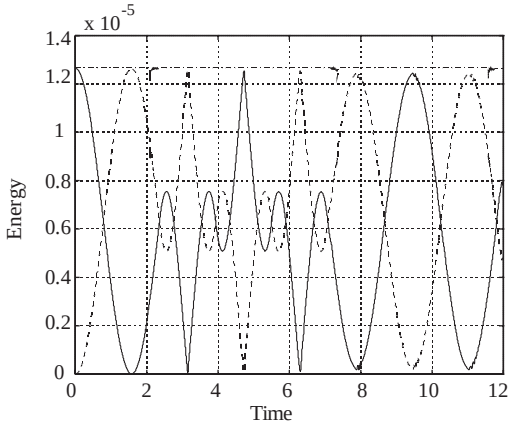

Fig. 5. Potential, kinetic, and total energy for $A_0 = 0.01$, $l/L = 1.05$, $h = 0.005$, $\gamma = 10^8$, and $N = 401$: —, potential; − −, kinetic, − · −, total energy.

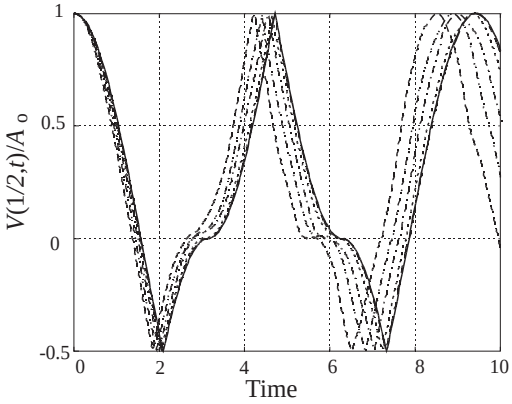

Fig. 6. Normalized vertical displacement of the midpoint, $V(\frac{1}{2}, t)/A_0$, where $G = 0$, $l = 1.05$, $h/A_0 = \frac{1}{2}$, and $A_0 = 0.01$, 0.03, 0.05, 0.07, and 0.09. The analytical solution of Cabannes for a linear string is plotted as a solid line: —, Cabannes; - -, $A_0 = 0.09$.

3.2. *Effects of large amplitude—no gravity*

We will now increase the amplitude of the initial vertical displacement in order to explore the geometrical non-linearity due to large amplitude. We vary the amplitude from 0.01 to 0.09 with 0.02 increments. We let $l = 1.05$, and $h/A_0 = \frac{1}{2}$. The midpoint displacements, normalized by the amplitudes, are shown in Fig. 6. The shapes of the responses are similar, but the response is faster when the amplitude is greater. This is similar to what occurs for free vibration without the obstacle in air.

We can find the frequency from the inverse of the time it takes to complete one cycle (near 3π in these cases). Alternatively, we can compute the frequency comparing the times to the first two impacts of a cable with those of a taut string. The latter has the advantages that it can be

Table 1
Period and frequency when the amplitude is varied in the absence of gravity

A_0	0.01	0.03	0.05	0.07	0.09
t_1	2.09	2.06	2.01	1.95	1.86
ω, $2.09/t_1$	1.00	1.01	1.04	1.07	1.12
t_2	7.32	7.24	7.08	6.85	6.52
ω, $(7.33-2.09)/(t_2-t_1)$	1.00	1.01	1.04	1.07	1.12

computed before significant numerical error accumulates, and it can be defined even for aperiodic motions.

We will denote the times to the first and the second contact as t_1 and t_2. The analytical solution obtained by Cabannes gives us 2.09 and 7.33 for the times to the first and the second contact, respectively. t_1 and t_2-t_1 obtained for different amplitudes are normalized by these analytical results and then inverted to give the frequency ratios. The frequency ratio, t_{1taut}/t_1, gives a very good approximation to the in-air natural frequency, ω_1, because the cable has not interacted with the obstacle until t_1.

The periods and the angular frequencies obtained using t_1 are shown in Table 1. The frequency ratio, $2.09/t_1$, tells us something about the cable itself due to its own non-linearity (such as geometrical non-linearity due to large amplitude) and independent of the obstacle. The frequency, $(7.33-2.09)/(t_2-t_1)$, on the other hand, tells us something about the frequency variation due to the interaction with the obstacle in addition to effects of its own non-linearity. In our case, the two frequencies are identical at least to the second decimal place. This suggests that, for $G=0$, Cabannes's results hold with respect to the free natural frequency which is modified solely by the cable non-linearity due to large amplitude [2].

3.3. *Effects of varying amplitude with gravity*

In this section, the effect of varying the initial amplitude of the vertical displacement in the presence of gravity on a nearly taut string is investigated. We will limit the range of amplitudes to a "small" amplitude in order to isolate the effects of gravity from the geometrical non-linearity due to the large amplitude explored in the previous section. The reason that we do not consider the large amplitude vibration is that as amplitude increases, the effects of gravity becomes small (the sag caused by the gravity is negligible compared to the amplitude of vibration), and the responses become similar to the ones without gravity that were investigated in Section 3.2. It should be noted that the terms "small" and "large" are somewhat imprecise. We will define a large amplitude as one that will modify the frequency by more than 1%, and we will denote it as A_{large}. It should also be noted that A_{large} depends on l. If gravity is included, A_{large} also depends on G.

When the amplitude is small, we found that the first natural frequency stays roughly at 1 in the absence of gravity (see previous section). However, we will find that this is not the case in the presence of gravity. Here, we will consider two cases. The first case is when the sag is insignificant

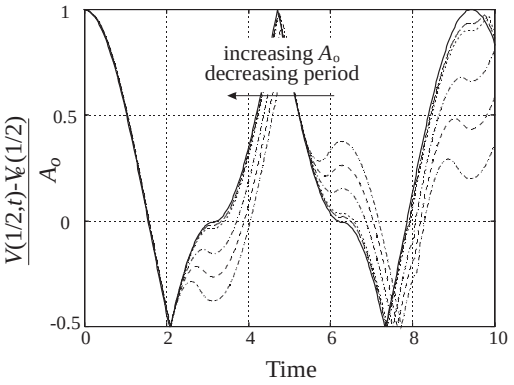

Fig. 7. Normalized dynamic vertical displacement at the midpoint where $G = 0.0001$, $l = 1.05$, $h/A_0 = \frac{1}{2}$, $A_0 > d$, and $A_0 = 0.0003$, 0.0005, 0.001, 0.005, and 0.01: $-$, $G = 0$.

compared to the amplitude but still smaller than A_{large} ($d < A_0 < A_{large}$), and the second case is when the sag is much larger than the amplitude, $A_0 \ll d$.

We let $G = 0.0001$, $l = 1.05$, and $h/A_0 = \frac{1}{2}$. The values of G and l are such that the cable is essentially a taut string ($\lambda^2 = 6.46 \times 10^{-5}$ and $d = 0.000024$). From Table 1, we see that, for $l = 1.05$, amplitudes greater than 0.01 are considered large. A relatively taut string (i.e., $\lambda^2 \approx 0$) is used here so that we can explore the dynamic behavior when the amplitude is greater than the sag. A stable solution was difficult to obtain for a cable with a large λ^2.

3.3.1. *Insignificant sag, $d < A_0 < A_{large}$*

The dynamic vertical displacements at the midpoint are shown in Fig. 7 for $A_0 = 0.0003$, 0.0005, 0.001, 0.005, and 0.01. These values are chosen so that they are still much greater than the sag, yet small enough so that the geometrical non-linearity due to large amplitude is small. We should keep in mind that when the obstacle is removed, the responses should look identical to that of a linear taut string. This can be verified by the fact that the responses in Fig. 7 before the first impact are identical.

After the first impact, the responses deviate from Cabannes's analytical solution and are no longer periodic. As A_0 increases, the response approaches that of a linear taut string without gravity (Cabannes's analytical solution). Therefore, gravity becomes negligible as A_0 increases as mentioned previously. When the amplitude is smaller, it takes longer to hit the obstacle for the second time. In order to understand why this occurs, let us consider the distance between the cable in equilibrium and the obstacle. The distance varies from h at $X = \frac{1}{2}$ to $h + d$ at $X = 0$ and 1. Therefore, the average distance between the obstacle and the equilibrium position is greater than h resulting in slower responses. As A_0 increases, the variation in the distance or the sag, d, is small compared to A_0. Therefore, as A_0 increases, the effect of the non-zero equilibrium position has a smaller effect on the overall dynamics. This is shown in Fig. 7 where the response corresponding to $A_0 = 0.01$ is close to the response of a linear taut string with no gravity.

As the amplitude is increased further, we expect that the effects of geometrical non-linearity will be more significant than the effects of gravity. Therefore, we expect that the responses to large

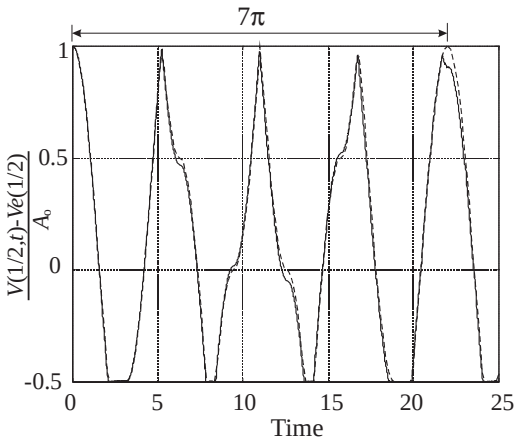

Fig. 8. Normalized dynamic vertical displacement at the midpoint corresponding to $G = 0.0001$, $l = 1.05$, $h/A_0 = \frac{1}{2}$, and $A_0 = 0.00001$. Cabannes's analytical solution for a point obstacle is plotted as a dotted line.

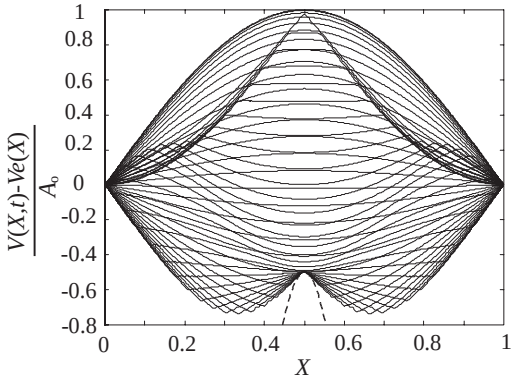

Fig. 9. Snapshots of dynamic vertical displacement normalized by the amplitude A_0 taken at $\Delta t = 1$ for $0 < t < 5.2$. Results correspond to $G = 0.0001$, $l = 1.05$, $h/A_0 = \frac{1}{2}$, and $A_0 = 0.00001$. The dotted line represents the obstacle.

initial amplitudes will be similar to those without gravity as shown in the previous section in Fig. 6.

3.3.2. *Significant sag, $A_0 \ll d$*

In this section, we will investigate the response when the sag is larger than the amplitude of vibration. Let us consider the responses for a very small A_0 so that the non-linear effects of large amplitude are not important. The solid line in Fig. 8 is the dynamic vertical displacement when $A_0 = 0.00001$. In this case, the cable seems to rest on the obstacle momentarily. In fact, results for a cable interacting with a straight obstacle are similar to the solution of a taut string interacting with a point obstacle. It is easier to see when the straight obstacle is viewed from the equilibrium position of the cable as shown (Fig. 9). The obstacle looks like a convex obstacle whose height is described by $-(h + d + V_e)/A_0$. The distance from the obstacle to the cable is greatest at the two ends of the cable and smallest in the middle. As A_0 becomes smaller, a smaller section of the cable

Table 2
Period and frequency with gravity for amplitudes smaller than A_{large}

A_0	0.00001	0.0003	0.0005	0.001	0.005	0.01
t_1	2.09	2.09	2.09	2.09	2.09	2.09
ω, $2.09/t_1$	1.00	1.00	1.00	1.00	1.00	1.00
t_2	7.86	7.73	7.62	7.50	7.37	7.35
ω, $(7.33-2.09)/(t_2-t_1)$	0.91	0.93	0.95	0.97	0.99	1.00

interacts with the obstacle. In the limit, the straight obstacle acts as a point obstacle. Cabannes [20] showed for a point obstacle that the motion of a string is periodic if the ratio h/A_0 is rational, and the period is $(3q-p)T_n/2$, where $h/A_0 = p/q$. h is positive upward, and T_n is the period of a free string. In this case when the obstacle is placed a distance of $A_0/2$ below the cable so that $p=-1$, $q=2$ and the period is 7π. Cabannes's solution in Fig. 8 repeats itself after $t=7\pi$. Note that the numerical solution becomes increasingly inaccurate with time due to numerical instability associated with the stiff obstacle.

It was shown by Cabannes [19] that a persistent contact (for a linear taut string without gravity) is possible only when the obstacle is convex with respect to the string. However, it is easy to show that, when gravity is included, a persistent contact is possible for a straight obstacle and also for a concave obstacle as long as the obstacle is placed below the string. To see this, we examine the equation of motion in the vertical direction (Eq. (22)) with distributed reaction force, R (acting in the positive vertical direction), given by

$$m\ddot{V} - (\varepsilon V')' + G - R = 0. \tag{29}$$

Persistent contact ($\ddot{V}=0$) is possible if and only if the reaction force is positive (normal to the obstacle) or

$$-(\varepsilon V')' + G > 0, \quad -(\varepsilon' V' + \varepsilon V'') + G > 0. \tag{30}$$

For a straight obstacle, $V' = V'' = 0$. G is positive, and therefore, it is possible to have a persistent contact. Note that if the obstacle is placed above the cable, we require R to be negative. This cannot be satisfied, and therefore, a persistent contact is impossible.

The analytical solution of Cabannes [20] with a point obstacle (placed at $X=\frac{1}{2}$ and $y=-A_0/2$) is also plotted in Fig. 8. The two responses are quite similar, and therefore, we can conclude that the straight obstacle acts as a point obstacle if the amplitude of vibration is very small.

We find that the variation in the frequency for amplitudes less than A_{large} ($A_0 < A_{large}$) is mainly due to the change in the effective shape of the obstacle (e.g., the straight obstacle acts as a convex obstacle for $d < A_0 < A_{large}$ and a point obstacle for $A_0 \ll d$). For $A_0 > A_{large}$, the obstacle behaves as a straight obstacle, and the variation in the frequency is mainly due to the geometrical non-linearity caused by large amplitude.

As a summary, Table 2 shows the normalized frequencies obtained from the time that the first two contacts occurred for both cases of insignificant and significant sag. By combining the results with the case of a large amplitude vibration in Table 1, we can show that the variation in the frequency for a wide range of A_0 after the contact has occurred (Fig. 10).

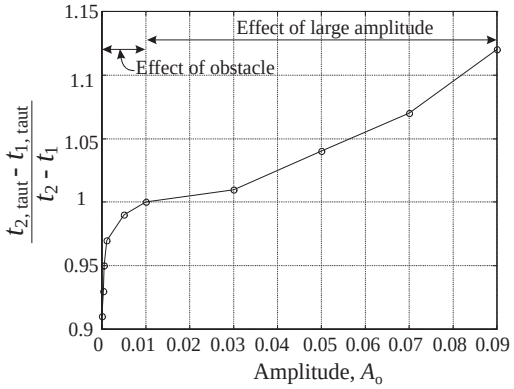

Fig. 10. The variation in the natural frequency after the impact for $l = 1.05$. Data are given in Tables 1 and 2.

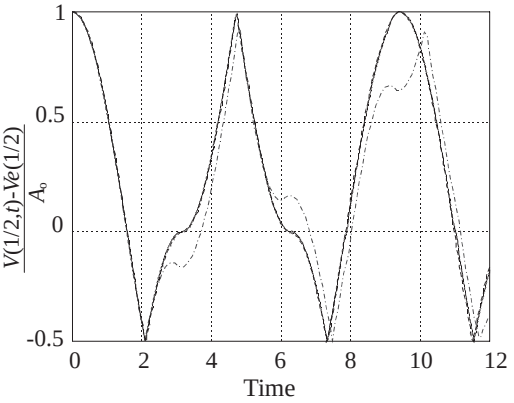

Fig. 11. Normalized dynamic vertical displacement interacting with straight and curved obstacles for $A_0 = 0.001$, $l = 1.05$, and $G = 0.0001$: $-$, curved obstacle, $- \cdot -$, straight obstacle; $- -$, $G = 0$ with a straight obstacle.

3.3.3. *Periodic response*

Naturally, we ask under what conditions the response is periodic for all A_0 just as in the case of a linear taut string without gravity. One circumstance is when the obstacle assumes the shape of the equilibrium configuration. That is, the depth of the obstacle is $y_{obstacle} = V_e(X) - h$. Fig. 11 shows the dynamic vertical displacement at the midpoint when such a curved obstacle is placed below the equilibrium position. For comparison, the vertical displacements with a straight obstacle with and without gravity are also plotted. Again, we used $A_0 = 0.001$ and $l = 1.05$. We find that when a curved obstacle is used, the periodicity is recovered.

This is possible because the cable is essentially a taut string. The linear taut string equations can be recovered by assuming that

$$U' \ll 1, \quad V'^2 \ll U'. \tag{31}$$

Then the strain in Eq. (4) is reduced to

$$\varepsilon = U'. \tag{32}$$

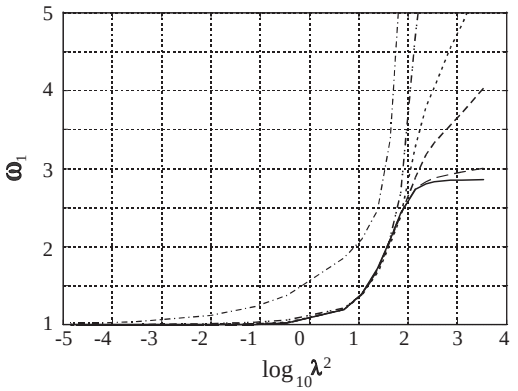

Fig. 12. Approximation to ω_1 using the assumed mode method. They are shown as functions of $\log_{10}\lambda^2$: —, $A_0 = 0.0001$ and Irvine and Caughey's result [9]; — —, $A_0 = 0.001$; – –, $A_0 = 0.003$; - -, $A_0 = 0.005$; – · ·–, $A_0 = 0.01$; – · –, $A_0 = 0.03$.

Then, the longitudinal equation of motion (21) becomes

$$m\ddot{U} - U'' = 0. \tag{33}$$

In addition, we let $\varepsilon = \varepsilon_d + \varepsilon_e$, where ε_d is the dynamic strain and ε_e is the equilibrium strain. It is reasonable to assume that the dynamic strain is negligible compared to the equilibrium strain, and the equilibrium strain is constant (i.e., constant equilibrium tension). Then, the vertical equation of motion (22) is reduced to

$$m\ddot{V} - \varepsilon_e V'' + G = \gamma(y_{obstacle} - V)^2. \tag{34}$$

By writing $V = V_d + V_e$ and $y_{obstacle} = V_e(X) - h$, we find that

$$m\ddot{V}_d - \varepsilon_e V_d'' = \gamma(h - V_d)^2. \tag{35}$$

Therefore, by assuming that the shape of the obstacle mirrors the equilibrium configuration of the cable, we were able to recover the equation of motion of a linear taut string vibrating against a straight obstacle without gravity.

Note that the same analysis cannot be applied to a cable with a large λ^2. In that case, the response will not be periodic even if the obstacle takes the shape of the equilibrium configuration.

3.4. *Effects of varying λ^2 on a shallow-sag cable*

In Section 3.3, we investigated the effect of amplitude on a nearly taut string with and without gravity. In this section, we wish to study the effect of λ^2 on a shallow-sag cable with small amplitudes. It was mentioned earlier that the amplitude is considered small if the variation in the natural frequency is also small. In order to find the range of amplitude that is considered small, we turn to the study conducted by Hagedorn and Schafer [5] and Takahashi and Konishi [6]. Hagedorn and Schafer investigated the amplitude dependence of the natural frequencies of a shallow-sag cable using the assumed mode method and Irvine and Caughey's mode shapes (Eq. (A.3)). Fig. 12 shows these approximations to the natural frequencies for a range of initial

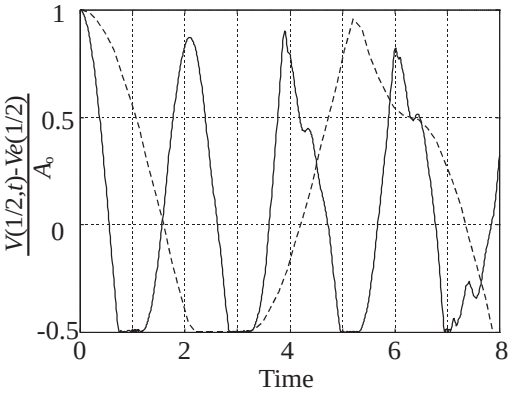

Fig. 13. Normalized dynamic vertical displacement at the midpoint where $G = 0.0001$, $h/A_0 = \frac{1}{2}$, and $A_0/d = 0.00115$: —, $l = 0.98$; – –, $l = 1.003$.

amplitudes (given in figure caption). The figure reveals that the natural frequencies are more sensitive to amplitude variations for cables with larger λ^2. In addition, Irvine and Caughey's results are valid for a very small amplitude vibration ($A_0 \leqslant 0.0001$). Therefore, in order to compare our findings with those of Irvine and Caughey, we will consider amplitudes less than or equal to 0.0001.

Even though Fig. 12 seems to suggest that the response only hardens (increasing frequency with increasing amplitude), this is not true in general. For a different range of amplitude, the frequency can also decrease with increasing amplitude. This is demonstrated in Fig. 6 of Ref. [6], where weak softening is observed for $0.0015 < d/l < 0.01$ and $H_e = 900$. Again, neither hardening nor softening effects are significant for amplitude less than 0.0001.

We first vary l from 0.98 to 1.003 and set $G = 0.0001$ and $h/A_0 = \frac{1}{2}$ and $\frac{1}{3}$. This range of l, between 0.98 and 1.003 with $G = 0.0001$, can produce λ^2 between 0.347 and 3.47×10^3 ($-0.46 \leqslant \log_{10} \leqslant 3.54$) and d/l always less than $1/8$.

For all cases, we will let the ratio $A_0/d = 0.00115$. In the previous section, we found that the ratio A_0/d determines how the obstacle behaves. For example, as the initial amplitude decreases, the straight obstacle behaves as a convex obstacle with decreasing radius of curvature. In the limit, the curvature will become very small so that the straight obstacle will behave as a point obstacle. As we vary λ^2, the sag varies. Therefore, if we keep the initial amplitude constant, the ratio A_0/d will also vary as the sag, d, varies. For all cases, we want the straight obstacle to behave the same way. Therefore, we keep the ratio A_0/d constant by varying the amplitude. The numerical value of the ratio A_0/d is determined from the cable with $l = 0.98$. A_0/d with $A_0 = 0.0001$ for this cable is 0.00115, and this value is used for all the other cables.

Fig. 13 shows a sample response when $l = 0.98$ and $l = 1.003$. In both cases, the responses are not periodic. We also notice that the time to the first impact is different. It takes longer for the cable with $l = 1.003$ to reach the obstacle. This is due to the fact that the first symmetric natural frequencies are modified according to Irvine and Caughey's result in Eq. (A.4). However, we will find that Irvine and Caughey's results alone cannot explain the differences that we see in the sample response. In this section, we attempt to explore where the additional discrepancies come

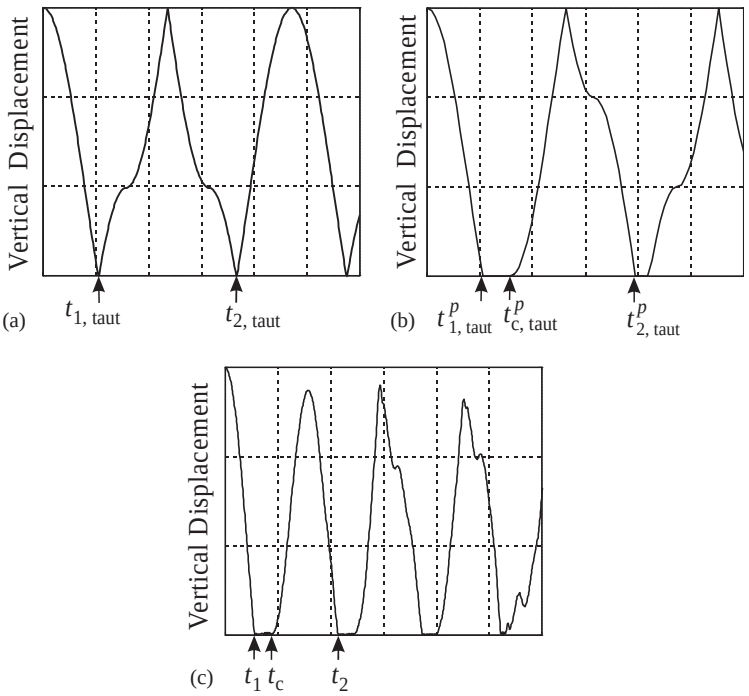

Fig. 14. Definitions of $t_{i,taut}$, $t^p_{i,taut}$, and t_i for $i = 1, 2$, or c. Linear taut string with (a) a straight obstacle and (b) a point obstacle. (c) cable with a straight obstacle.

from. It should be noted that numerical error builds up with each impact, and the response after two impacts is no longer smooth (solid line in Fig. 13).

We will report our results in terms of the times to the critical events, as we have done previously. To do so, let us reiterate the definitions of the critical times. We denote the first two times that a linear taut string comes in contact with the straight obstacle as $t_{1,taut}$ and $t_{2,taut}$ (Fig. 14(a)). Further, we denote the first two times that a linear taut string comes in contact with the point obstacle as $t^p_{1,taut}$ and $t^p_{2,taut}$ (Fig. 14(b)). In addition, $t^p_{c,taut}$ is the time that the cable leaves the point obstacle after the first contact. The times to the first contact with a straight obstacle and a point obstacle will always be the same (i.e. $t_{1,taut} = t^p_{1,taut}$). The first two times that a cable comes in contact with a straight obstacle are denoted as t_1 and t_2, and the time that the cable leaves the obstacle after the first contact is denoted as t_c (Fig. 14(c)).

First, we compare the time to the first contact (t_1) and the time between the first two contacts ($t_2 - t_1$) of a cable to those of a linear taut string with a straight obstacle. The frequency ratios, $t_{1,taut}/t_1$ and $(t_{2,taut} - t_{1,taut})/(t_2 - t_1)$, are plotted in Fig. 15. The first ratio, $t_{1,taut}/t_1$, should follow Irvine and Caughey's results closely since the cable has not yet interacted with the obstacle, and it does. However, the frequency ratio based on $(t_2 - t_1)$ does not. Instead, it produces frequency ratios that are slightly smaller than the frequencies obtained by Irvine and Caughey for all λ^2. The discrepancy comes partly from the fact that, for a cable, the obstacle no longer behaves as a straight obstacle, but as a point obstacle. This was previously demonstrated for the limiting case of a taut string with a small amplitude of vibration in Section 3.3.2, where we showed that the

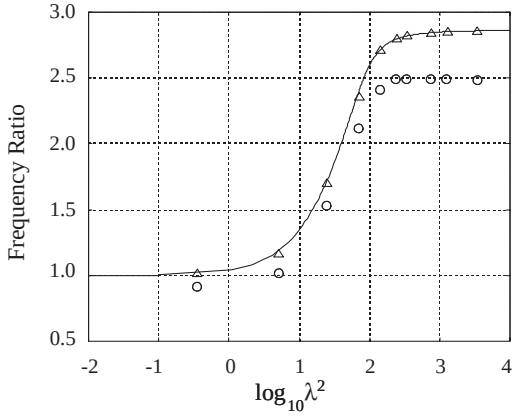

Fig. 15. The frequency ratios when $h/A_0 = \frac{1}{2}$: –, Irvine and Caughey; Δ, $t_{1,taut}/t_1$; o, $(t_{2,taut} - t_{1,taut})/(t_2 - t_1)$.

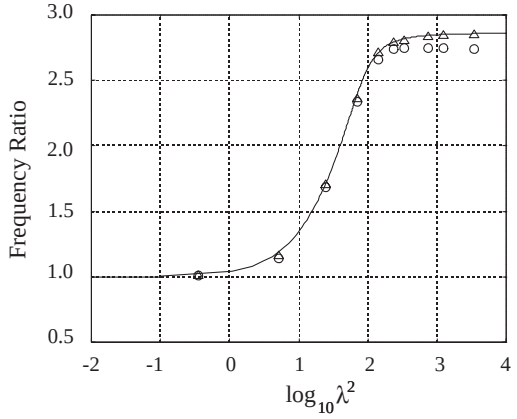

Fig. 16. The frequency ratios when $h/A_0 = \frac{1}{2}$: –, Irvine and Caughey; Δ, $t^p_{1,taut}/t_1$; o, $(t^p_{2,taut} - t^p_{1,taut})/(t_2 - t_1)$.

frequency ratio $(t_{2,taut} - t_{1,taut})/(t_2 - t_1)$ approached 0.91 (Table 2) as the amplitude decreased. This value agrees with the frequency ratio of the current case when $\lambda^2 = 0.347$ ($\log_{10}\lambda^2 = -0.46$) in Fig. 15. Does this mean that the discrepancy between $(t_{2,taut} - t_{1,taut})/(t_2 - t_1)$ and Irvine and Caughey's results can be explained only by the change in the effective shape of the obstacle (from straight to point obstacle)?

In an attempt to remove the influence of the effective shape of the obstacle, we compare our critical times with those of a taut string vibrating against a point obstacle whose response is shown as a dotted line in Fig. 8. For a taut string with a point obstacle located at $y = -A_0/2$, the critical times are $t^p_{1,taut} = 2.09$ (same as $t_{1,taut}$) and $t^p_{2,taut} = 7.86$. Fig. 16 shows the frequency ratios $t^p_{1,taut}/t_1$ and $(t^p_{2,taut} - t^p_{1,taut})/(t_2 - t_1)$. We find that the frequency ratio based on $t_2 - t_1$ agrees better with Irvine and Caughey's result for cables with smaller λ^2. For cables with larger λ^2, the frequency ratio, $(t^p_{2,taut} - t^p_{1,taut})/(t_2 - t_1)$, is still slightly smaller than the natural frequencies obtained by Irvine and Caughey. That is, the change in the effective shape of the obstacle alone cannot explain the reduction in the frequency ratio $(t_{2,taut} - t_{1,taut})/(t_2 - t_1)$.

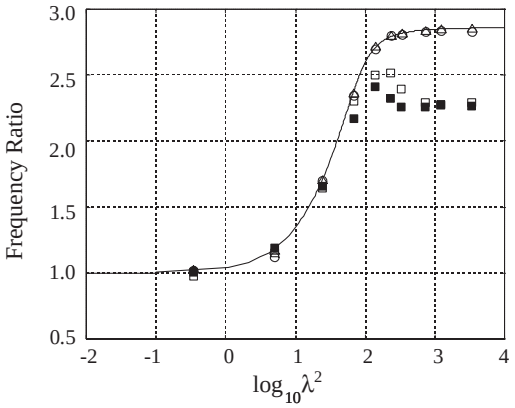

Fig. 17. The frequency ratios: –, Irvine and Caughey; Δ, $t^p_{1,taut}/t_1$; □ and ■, $(t^p_{c,taut} - t^p_{1,taut})/(t_c - t_1)$; o, $(t^p_{2,taut} - t^p_{c,taut})/(t_2 - t_c)$. The hollow symbols are used when $h/A_0 = \frac{1}{2}$ and the filled symbols are used when $h/A_0 = \frac{1}{3}$.

Table 3
Sets of l and G used in Fig. 18

l	0.610	0.678	0.752	0.833	0.913
G	0.0562	0.0428	0.0292	0.0160	0.0058
d/l	0.605	0.500	0.400	0.300	0.200
ψ_0	71.8°	67.4°	61.4°	52.7°	39.8°

We will continue to compare our results with those of a linear taut string with a point obstacle. In addition to t_1 and t_2, let us look at the time that the cable leaves the obstacle, $t^p_{c,taut}$ and t_c. Fig. 17 shows the frequency ratios, $t^p_{1,taut}/t_1$, $(t^p_{c,taut} - t^p_{1,taut})/(t_c - t_1)$, and $(t^p_{2,taut} - t^p_{c,taut})/(t_2 - t_c)$. The second frequency ratio is based on the time that the cable is in contact with the obstacle, and the third is based on the time that the cable is vibrating freely after the first contact and before the second contact. The figure shows that the frequency ratios follow Irvine and Caughey's results when the cable is not in contact with the obstacle (based on t_1 and $t_2 - t_c$). On the other hand, the frequency ratio calculated based on the time that the cable stays in contact with the obstacle (based $t_c - t_1$) is slightly reduced. This is an important result since it says that the cable behaves differently when it is in contact with the obstacle from when it is not. In other words, only the time that the cable is in contact with the obstacle is disproportionately increased for larger λ^2.

The filled symbols in Fig. 17 are the frequency ratio, $(t^p_{c,taut} - t^p_{1,taut})/(t_c - t_1)$, for $h/A_0 = \frac{1}{3}$. Similar behavior is observed in that the frequency ratio based on the amount of time that the cable stays with the obstacle is reduced for cables with large λ^2. For both $h/A_0 = \frac{1}{2}$ and $h/A_0 = \frac{1}{3}$, the reductions in the frequency ratio based on the contact time, $(t^p_{c,taut} - t^p_{1,taut})/(t_c - t_1)$, do not significantly differ.

3.5. Effect of sag-to-span ratio on cables with constant λ^2

We now investigate the effect of sag-to-span ratio on cables with $\lambda^2 = 595.7$ ($\log_{10}\lambda^2 = 2.775$). The values of l, G, d/l, and ψ_0 are given in Table 3. ψ_0 is the angle that the cable ends make with

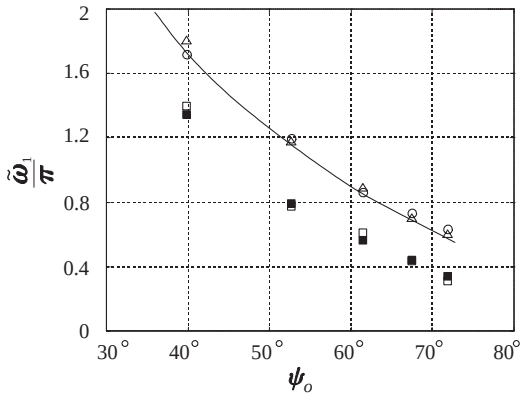

Fig. 18. The frequency ratios with varying d/l on a cable with $\log_{10}\lambda^2 = 2.775$: –, curve fit through experimental data; Δ, $t^p_{1,taut}/t_1$; □ and ■, $(t^p_{c,taut} - t^p_{1,taut})/(t_c - t_1)$; o, $(t^p_{2,taut} - t^p_{c,taut})/(t_2 - t_c)$. The hollow symbols are used when $h/A_0 = \frac{1}{2}$ and the filled symbols are used when $h/A_0 = \frac{1}{3}$.

the horizontal and is used as a measure of sag. For example, $\psi_0 = 0^\circ$ for a horizontal cable and $\psi_0 = 90^\circ$ for a hanging cable. Fig. 18 shows the frequency ratios based on t_1, $t_c - t_1$, and $t_2 - t_c$ as functions of ψ_0 for $h/A_0 = \frac{1}{2}$. The frequency ratios plotted here are $t^p_{1,taut}/t_1 \cdot \sqrt{H_e/Gl \tan(2\psi_0)}$, $(t^p_{c,taut} - t_{1,taut})/(t_c - t_1) \cdot \sqrt{H_e/Gl \tan(2\psi_0)}$, and $(t^p_{2,taut} - t^p_{c,taut})/(t_2 - t_c) \cdot \sqrt{H_e/Gl \tan(2\psi_0)}$.

In the same figure, the frequency ratios based on $(t_c - t_1)$ for $h/A_0 = \frac{1}{3}$ are plotted using the filled symbols. The experimental data by Rudnick et al. (reviewed in Ref. [14]) are also plotted as a solid line. Again, the contact time $(t_c - t_1)$ for both $h/A_0 = \frac{1}{2}$ and $\frac{1}{3}$ is disproportionately longer, therefore, reducing the frequency ratio. The percent reduction is larger for a cable with larger sag. However, it appears that the reduction in the frequency ratios is not significantly affected by the ratio, h/A_0.

4. Summary and conclusion

The equations of motion of a cable using the finite strain model and Hamilton's variational principle were derived. The model included horizontal as well as vertical displacement. The equations of motion and boundary conditions were normalized so that we were able to identify three factors that affect the response: the ratio of the span to the undeformed length of the cable, the ratio of the weight to the longitudinal stiffness, and initial conditions.

We showed that the current numerical scheme was adequate by comparing our results with Cabannes's analytical solution for a taut string vibrating against a straight obstacle. The total energy was plotted to show that it stayed relatively constant after the first two contacts with the obstacle.

We investigated the effect of varying the initial vertical amplitude, A_0, with zero initial velocities in the absence of gravity. The numerical solution to the fully non-linear equations motion showed that the periodicity seen in the analytical solution of a linear taut string was maintained, but the frequency increased with increasing amplitude.

Once gravity was included, it is found that the periodicity was lost even for a taut string. This periodicity was recovered when the obstacle took the shape of cable's equilibrium configuration. It was found that the ratio A_0/d determined how the straight obstacle behaved. For example, when the initial amplitude was much larger than the sag, the straight obstacle behaves as a straight obstacle. As the value of A_0/d decreased, the straight obstacle behaved as a convex obstacle with an decreasing radius of curvature. The behavior approached that of a point obstacle in the limit as A_0/d became small, and the analytical results of Cabannes for the linear taut string with a point obstacle could be used to predict the motion of the cable.

We explored the effect of varying curvature on a shallow-sag cable for $h/A_0 = \frac{1}{2}$ and $\frac{1}{3}$. The ratio A_0/d was kept constant at 0.00115 so that the obstacle would behave in a consistent manner as we varied the curvature. In all cases, the motion was no longer periodic. The times to the critical events such as the time to the first contact and the time between the first and the second contact (t_1 and $t_2 - t_1$) were monitored. The two frequency ratios were obtained by comparing these critical times to those of a taut string vibrating against a straight obstacle. It was found that the frequency ratios based on the time to the first impact followed Irvine and Caughey's results closely. However, the frequency ratios based on the time between the two impacts were smaller than the frequencies obtained by Irvine and Caughey for all λ^2. The discrepancy was greater for cables with larger λ^2. There were two reasons for this. The first was that the straight obstacle behaves as a point obstacle when the amplitude was very small. It was demonstrated that the time to the second contact for a point obstacle was larger than for a straight obstacle. The second reason was that the time that the cable stays in contact with the obstacle became disproportionately longer for a cable with a large λ^2. The reduction in the frequency ratio based on the contact time ($t_c - t_1$) was a function of λ^2 and sag to span ratio. However, it did not appear that the ratio h/A_0 had a considerable impact on the frequency ratios. The same analysis was performed on an inextensible deep-sag cable for $h/A_0 = \frac{1}{2}$ and $\frac{1}{3}$. For all values of sag we used, only the frequency ratios based on $t_c - t_1$ were reduced. Again, it appeared that the ratio h/A_0 did not have a considerable impact on the frequency ratios.

Acknowledgements

We gratefully acknowledge the support of the Office of Naval Research Code 3210E (Ocean Engineering and Marine Systems), grant number N00014-92-J-1269. Support for the first author was also provided by a Woods Hole Oceanographic Institution postdoctoral fellowship.

Appendix A. Previous studies by Irvine and Caughey, and Saxon and Cahn

In this section, the mode shapes and the frequency equation for symmetric modes obtained by Irvine and Caughey for a shallow-sag cable and those for an inextensible cable by Saxon and Cahn are listed.

A.1. Irvine and Caughey's results

Here, we will present the symmetric mode shapes and the frequency equation for a shallow-sag cable. Irvine and Caughey [9] studied the effect of gravity on a shallow-sag cable. Their results are

expressed in terms of λ^2 and d/l, where λ^2 is defined by

$$\lambda^2 = \frac{(m^* g^* l^*)^2 E^* A_0^*}{H_e^{*3}} \frac{l^*}{L_e^*}, \tag{A.1}$$

where $L_e^* = \int_0^{l^*} (1 + (\partial V_e^*/\partial x^*)^2)^{3/2}\, \mathrm{d}x^*$. In terms of variables in this paper, λ^2 is given by

$$\lambda^2 = \frac{G^2}{H_e^3} \frac{l^*}{L_e^*}. \tag{A.2}$$

λ^2 represents the ratio of elastic to geometrical stiffness. If λ^2 is large, the cable acts as an inextensible cable such that it will rearrange itself geometrically to achieve a certain shape of vibration. If λ^2 is small, the cable will achieve the same effects by extending.

Irvine and Caughey found that the nth symmetric mode shapes are given by

$$V_n(X) = \frac{1 - \tan(\boldsymbol{\omega}_n/2)\sin(\boldsymbol{\omega}_n X) - \cos(\boldsymbol{\omega}_n X)}{1 - 1/\cos(\boldsymbol{\omega}_n/\mathbf{2})}.$$

$$\begin{aligned} U_n(X) = {} & 8\frac{d}{l}\frac{1}{1 - 1/\cos(\boldsymbol{\omega}_n/\mathbf{2})} \\ & \times \left\{ \frac{\boldsymbol{\omega}_n^2 l}{\lambda^2 L_e}\left(X + 24\left(\frac{d}{l}\right)^2 (X - 2X^2 + 4X^3/3)\right) \right. \\ & - \tfrac{1}{2}(1 - 2X)\left(1 - \tan\frac{\boldsymbol{\omega}_n}{2}\sin\boldsymbol{\omega}_n X - \cos\boldsymbol{\omega}_n X\right) \\ & \left. - \frac{1}{\boldsymbol{\omega}_n}\left(\boldsymbol{\omega}_n X - \tan\frac{\boldsymbol{\omega}_n}{2}(1 - \cos\boldsymbol{\omega}_n X) - \sin\boldsymbol{\omega}_n X\right)\right\}, \end{aligned} \tag{A.3}$$

where $\boldsymbol{\omega}_n$ satisfies the characteristic equation given by

$$\tan\frac{\boldsymbol{\omega}_n}{2} = \frac{\boldsymbol{\omega}_n}{2} - \frac{4}{\lambda^2}\left(\frac{\boldsymbol{\omega}_n}{2}\right)^3. \tag{A.4}$$

Note that Irvine and Caughey's natural frequencies are related to our natural frequencies by $\boldsymbol{\omega}_n = \pi\omega_n$.

A.2. Saxon and Cahn's results on an inextensible cable

Here, we present the symmetric mode shapes and the frequency equation for an inextensible cable. Saxon and Cahn [14] found that the nth symmetric mode shapes are given by

$$\begin{aligned} u_n(\psi) &= \cos(\tilde{\omega}_n f + g/\tilde{\omega}_n)\cos^{1/4}\psi - \frac{\cos(\tilde{\omega}_n f(\psi_0) + g(\psi_0)/\tilde{\omega}_n)}{\cos_0^{3/4}\psi_0}\cos\psi, \\ v_n(\psi) &= \sin(\tilde{\omega}_n f + g/\tilde{\omega}_n)\frac{\cos^{1/4}\psi}{\tilde{\omega}_n} - \frac{\cos(\tilde{\omega}_n f(\psi_0) + g(\psi_0)/\tilde{\omega}_n)}{\cos_0^{3/4}\psi_0}\sin\psi, \end{aligned} \tag{A.5}$$

where u_n and v_n are the nth symmetric mode shapes of the normal and tangential (along the cable) displacements, ψ is the angle that the cable (in equilibrium) makes with the horizontal, ψ_0 is the

angle that the cable makes with the horizontal at the fixed end, f and g are defined as

$$f(\psi) = \int_0^{\psi} \frac{1}{\cos^{3/2}\bar{\psi}}\,\mathrm{d}\bar{\psi},$$

$$g(\psi) = \frac{11}{8}\int_0^{\psi} \left\{\left(1 + \tfrac{1}{44}\tan^2\bar{\psi}\right)\cos^{3/2}\bar{\psi}\right\}\mathrm{d}\bar{\psi}, \tag{A.6}$$

and $\tilde{\omega}$ satisfies the frequency equation given by

$$\cot(\tilde{\omega}f(\psi_0) + g(\psi_0)/\tilde{\omega}) = \frac{1}{\tilde{\omega}}\frac{\cos^{5/2}\bar{\psi}_0}{\sin\bar{\psi}_0}. \tag{A.7}$$

The mode shapes of the vertical and horizontal displacements are obtained by transforming the co-ordinate system such that

$$\begin{bmatrix} U_n(\psi) \\ V_n(\psi) \end{bmatrix} = \begin{bmatrix} -\sin\psi & \cos\psi \\ -\cos\psi & -\sin\psi \end{bmatrix}\begin{bmatrix} u_n(\psi) \\ v_n(\psi) \end{bmatrix}, \tag{A.8}$$

and ψ can be written such that

$$\psi = \tan^{-1}\frac{-\mathrm{d}V_e}{\mathrm{d}X + \mathrm{d}U_e}. \tag{A.9}$$

The last equation gives us the relationship between ψ and X so that the mode shapes can be expressed in terms of X instead of ψ.

Appendix B. Nomenclature

Dimensional variables

A_0^* cross-sectional area of the reference cable, m^2
d^* sag, m
E^* Young's modulus, N/m^2
h^* distance between the obstacle and the cable, m
H_e^* horizontal component of the tension, N
KE^* kinetic energy, N m
L^* length of the undeformed cable, m
l^* span, the distance between the two ends, m
m^* mass per unit undeformed length, kg/m
m_x^* mass per unit horizontal length, kg/m
PE^* potential energy, N m
p_u^* horizontally distributed load, N/m
p_v^* vertically distributed load, N/m
t^* time, s
t_1^* the time to the first impact, s
t_2^* the time to the second impact, s
TE^* total energy, N m

U^* horizontal displacement, m
U_e^* static horizontal displacement, m
V^* vertical displacement, m
V_e^* static vertical displacement, m
X^* Lagrangian co-ordinate, m
x^* Eulerian co-ordinate, m
ε_{ij}^* Green's strain
σ_{ij}^* the second Piola–Kirchhoff stress, N/m^2
ω_1^* the first symmetric natural frequency, rad/s
$\bar{\omega}_1^*$ ω_1^* of a linear taut string, rad/s

Nondimensional variables

A_0 A_0^*/L^{*2}
d d^*/L^*
G $m^*g^*L^*/E^*A_0^*$
h h^*/L^*
H_e $H_e^*/E^*A_0^*$
KE $KE^*/E^*A_0^*L^*$
l l^*/L^*
m $m^*L^{*2}\bar{\omega}_1^2/E^*A_0^*$
PE $PE^*/E^*A_0^*L^*$
p_u $p_u^*L^*/E^*A_0^*$
p_v $p_v^*L^*/E^*A_0^*$
t $t^*\bar{\omega}_1^*$
t_i $t_i^*\bar{\omega}_1^*$
TE $TE^*/E^*A_0^*L^*$
U U^*/L^*
U_e U_e^*/L^*
V V^*/L^*
V_e V_e^*/L^*
X X^*/L^*
x x^*/L^*

References

[1] H. Cabannes, Mouvements d'une corde vibrante en presence d'un obstacle rectiligne, *C. R. Acad Sci. Paris, Series II* 295 (1982) 637–640.
[2] G.F. Carrier, On the nonlinear vibration problem of the elastic string, *Quarterly Journal of Applied Mathematics* 3 (2) (1945) 157–165.
[3] G.F. Carrier, A note on the vibrating string, *Quarterly Journal of Applied Mathematics* 7 (1) (1949) 97–101.
[4] C. Truesdell, Outline of the history of flexible or elastic bodies up to 1788, *Journal of Acoustical Society of America* 32 (1960) 1647.
[5] P. Hagedorn, B. Schafer, On non-linear free vibrations of an elastic cable, *International Journal of Nonlinear Mechanics* 15 (1980) 333–340.

[6] K. Takahashi, Y. Konishi, Non-linear vibrations of cables in three dimensions, Part I: non-linear free vibrations, *Journal of Sound and Vibration* 118 (1) (1987) 69–84.
[7] A. Simpson, Determination of the inplane natural frequencies of multispan transmission lines by a transfer matrix method, *Proceedings of the IEEE* 113 (5) (1966) 870–878.
[8] H.H. West, L.F. Geschwindner, Natural vibrations of suspension cables, *Journal of the Structural Division ST11* (1975) 2277–2291.
[9] H.M. Irvine, T.K. Caughey, The linear theory of free vibrations of a suspended cable, *Proceedings of the Royal Society London* A341 (1974) 299–315.
[10] J.H. Rohrs, On the oscillations of a suspension cable, *Philosophical Society* 9 (1851) 379–398.
[11] M.S. Triantafyllou, The dynamics of taut inclined cables, *Quarterly Journal of Mechanics and Applied Mathematics* 37 (3) (1984) 421–440.
[12] E.J. Routh, Fifth Edition, Dover Publications, New York, 1892, re-issued 1945.
[13] A.G. Pugsley, On the natural frequencies of suspension chains, *Quarterly Journal of Mechanics and Applied Mathematics* 2 (4) (1949) 412–418.
[14] D. Saxon, A.S. Cahn, Modes of vibration of a suspended chain, *Quarterly Journal of Mechanics and Applied Mathematics* 6 (3) (1953) 273–285.
[15] N.C. Perkins, C.D. Mote, Three-dimensional vibration of traveling elastic cables, *Journal of Sound and Vibration* 114 (2) (1987) 325–340.
[16] S.M. Han, H. Benaroya, Nonlinear coupled transverse and axial vibration of a compliant structure 1: formulation and free vibration, *Journal of Sound and Vibration* 237 (5) (2000) 837–873.
[17] E.J. Dean, R. Glowinski, Y.M. Kuo, M.G. Nasser, Technical Report, UH/MD80, University of Houston Research Report, 1990.
[18] H.M. Irvine, *Cable Structures*, Dover, New York, 1981.
[19] H. Cabannes, Cordes vibrantes avec obstacles, *Acoustica* 55 (1984) 14–20.
[20] H. Cabannes, Mouvements d'une corde vibrante en presence d'un obstacle ponctuel fixe, *C. R. Acad. Sci. Paris, Series II* 298 (1984) 613–616.